SCSU Journal of Student Scholarship

Volume 1
Issue 1 *Special Issue: 9th Annual Minnesota State Conference of Undergraduate Scholarly and Creative Activity*

Article 1

October 2020

# Laser Production and Characterization of Zinc-Oxide Nanoparticles

Bijaya Ghorasainee
*St. Cloud State University*

Sanjeev Regmi
*St. Cloud State University*

John Sinko
*St. Cloud State University*

MINNESOTA UNDERGRADUATE SCHOLARS
Proceedings of the 9th Annual Minnesota State Conference of Undergraduate Scholarly and Creative Activity
and
St. Cloud State University Journal of Student Scholarship, Vol. 1, Special Issue 1, 2020
MINNESOTA STATE

# Laser Production and Characterization of Zinc Oxide Nanoparticles

Bijaya Ghorasainee[1], Sanjeev Regmi[1], and John E. Sinko[2]

[1]*Department of Mechanical Engineering, St. Cloud State University, St. Cloud, MN 56301*
[2]*Department of Physics & Astronomy, St. Cloud State University, St. Cloud, MN 56301*

## Abstract

ZnO nanoparticles exhibit attractive optical properties that are important in the realm of catalysis and nanotechnology involving the developments of solar cells, chemical sensors and other optoelectronic devices. The main objective of this project was to create zinc oxide nanoparticles of less than 10 nm size by using an Nd: YAG laser and characterize the particle diameter. Zinc oxide nanoparticles were prepared by vaporizing zinc in neat deionized water by laser ablation, aided by a physical 2D-motional micro-stage programmed by Arduino. The addition of surfactant was explored to reduce aggregation of the nanoparticles. Various purification methods were applied to this process, including filtration and centrifugation, to reduce aggregation and improve the purity of zinc oxide nanoparticles. The ablated zinc oxide nanoparticles were analyzed with Dynamic Light Scattering (DLS), Scanning Electron Microscopy (SEM) with Energy Dispersal Spectroscopy (SEM/EDS) and Optical Profilometry (OP). The measured diameter of the nanoparticles is found at around 30-100 nm, with a peak around 35 nm, as analyzed by DLS method. Optical Profilometry allows estimation of thickness of ZnO films, while the elemental composition and large particle sizes can be detected by SEM/ EDS. We tested energy intensity, spot size, spot size overlap, and laser focusing setup of Zno nanoparticles. Future research will mainly focus on creating smaller Zinc Oxide nanoparticles i.e. (10±1) nm by the effective use of surfactant and purification methods.

## Introduction

Nanoparticles – particles of less than 100nm diameter – have interesting chemical, biological and optical properties that change as their size approaches the atomic level, compared to bulk material with the same composition. Such particles have widespread potential in medical applications, as well as for food packaging materials in order to inhibit the growth of food pathogens. In choosing a specific nanoparticle species, toxicity is a strong factor for consideration.

For this study, we chose to produce zinc oxide nanoparticles, which are nontoxic for humans, but toxic for aquatic organisms. Bulk ZnO is a stable material, with a melting point of 2248 K [1(a)]. Zinc oxide nanoparticles have been widely investigated as a photo-emissive material because nanocrystallization can enhance the optical and electrical properties of wide band gap semiconductors by the quantum confinement effect [2]. Zinc oxide nanoparticles are transparent in the visible range of the electromagnetic spectrum but can act as a physical filter for solar ultraviolet (UV) radiation. Photochemically, ZnO has a relatively low band energy of 3.37eV and an even lower excitation energy of 60meV, which has triggered

extensive research on the properties of ZnO and the production of nanoparticles using physical and chemical methods [3]. The ultimate purpose of this project is to produce nanoparticles of <10nm in order to permit an experimental test of a theory of Dr. Christofer Nelson, Department of Physics & Astronomy, St. Cloud State University, related to quantum effects on the glass transition in semiconductors [4].

One method under development for production of nanoparticles is laser ablation: violent removal of material by intensely irradiating a surface with a laser beam [5]. One method for creating nanoparticles, described in the literature, is laser ablation of metallic zinc immersed in deionized water [6,7]. This approach has several advantages including technical simplicity and chemical pureness, compared to other methods such as plasma-enhanced chemical vapor deposition or ball milling [3]. The most important advantage of the laser ablation method is that nanoparticles can be prepared directly from a pure zinc surface. In principle, production of a narrow size distribution of particles at atmospheric pressure and without post processing is possible. However, steps to limit excessive coalescence and aggregation of nanoparticles were often undertaken in the literature, including the use of surfactant molecules such as Tween 80, because nanoparticles prepared in deionized water evinced a wide size distribution [8].

Direct vaporization- or plasma-based ablation is described by Stafe as indicated:

$$F_{th} = 2H_v\sqrt{\frac{\rho\kappa\tau}{C_p}}, \qquad (1)$$

where $H_v$ is the latent heat of vaporization, $\rho$ is the material density, $C_p$ is the heat capacity at constant pressure, $\kappa$ is the thermal conductivity, and $\tau$ is the laser pulse duration.

The threshold for melting-based laser ablation of metallic samples was described by Stafe as a fluence, meaning energy per area: [5]

$$F_{th} = \frac{2(T_m - T_0)\sqrt{\rho C_p \kappa\tau}}{1-R}, \qquad (2)$$

where $T_m$ is the melting point, $T_0$ is the ambient temperature, and $R$ is the surface reflectance.

Surface reflectance can be calculated at normal incidence (beam perpendicular to the surface) in air using the Fresnel equation for metals, with a complex index of refraction $n = n_r + in_i$ [9]:

$$R = \frac{(1-n_r)^2 + n_i^2}{(1+n_r)^2 + n_i^2} \qquad (3)$$

Relevant optical constant values are organized in Table 1, including theoretical density functional theory (DFT) predictions and experimental reflection electron energy loss spectroscopy (REELS) data for the optical constants of zinc metal, as well as power reflectance $R$, which was calculated from these values using Equation (3) [10]:

Table 1: Optical constants and reflectance of zinc at 1064nm [10]

| $n_r$ | | $n_i$ | | $R$ | |
|---|---|---|---|---|---|
| Theory | Experiment | Theory | Experiment | Theory | Experiment |
| 4.230 | 2.885 | 4.657 | 6.289 | 0.655 | 0.789 |

These theoretical and experimental data will allow us to predict the ablation threshold for zinc. The necessary thermal data from the literature is organized in Table 2, where *m* is molar mass:

Table 2: Thermodynamic parameters of zinc metal

| Parameter: | $m$ | $T_m$ | $T_b$ | $\rho$, 298 K | $C_p$, 298 K, avg. | $H_v$ | $\kappa$, 298 K |
|---|---|---|---|---|---|---|---|
| Units: | g/mol | K | K | kg/m$^3$ | J/(kg K) | J/kg | W/(K m) |
| Value: | 65.38 | 693 | 1180 | 7133 | 386 | $1.99\times10^6$ | 116 |
| Source: | [1(b)] | [1(b)] | [1(b)] | [1(b)] | [1(c)] | [11] | [1(d)] |

The maximum achievable fluence is determined from the diffraction-limited minimum spot size for a stigmatic Gaussian beam:

$$d = \frac{2.44\, f\, \lambda}{D}, \qquad (4)$$

where $d$ is the spot diameter, $f$ is the focal length of the lens, $\lambda$ is the wavelength, and $D$ is the effective collimated beam diameter that is focused by the lens.

Next, the equipment and methods of the experiment will be described.

## Experiment and Methods

### *I. Creation of ZnO Nanoparticles*

In order to produce zinc oxide nanoparticles, a 500 μm-thick 99.95% pure zinc foil was constrained at the bottom of a beaker filled with deionized water until the metal rested 16mm below the surface. A 2-axis motional stage was built by the first two authors using two CD-ROM motors and was controlled by an Arduino program using code designed and created by the same authors. A 1 mW Helium-Neon laser beam with a wavelength of 633nm was used to illuminate the target spot on the sample. Then a Nd:YAG laser (Continuum YG-660) operating at $\lambda$ = 1064 nm, with frequency of 10 Hz, 100 mJ pulse energy, and pulse duration of 90 μs, was used to ablate the sample. The high energy laser beam was passed through a lens with focal length 250mm and then focused onto the piece of zinc metal.

We first estimated the threshold for ablation, assuming a vaporization-driven process. Using the data from Table 2 in Equation (1), that vaporization threshold is predicted to be $F_{th} \approx 175$ J/cm$^2$. On the other hand, if the process is dependent on only melting the zinc surface, we can use Equation (2) with $T_0$ =295 K, the average ambient temperature in our laboratory. In that case, we calculate $F_{th} \approx 39$ J/cm$^2$ if the DFT calculation is to be trusted, or $F_{th} \approx 64$ J/cm$^2$ if the experimental REELS data is accurate. The next step is to see if these fluence limits are achievable. Using Equation (3) with input values of $D$ = 8 mm, $f$ = 250 mm, and $\lambda$ = 1064 nm, we predict a minimum spot diameter of around 80μm, or for which the beam fluence could reach up to 1934 J/cm$^2$, well in excess of the ablation threshold. Based on the lowest estimate of $F_{th}$ (39 J/cm$^2$), we would expect the maximum spot diameter where ablation could still be achieved to be around 570 μm.

As a result of the irradiation of the Nd:YAG laser beam onto the zinc surface, the high energy laser pulse vaporizes the zinc into a plasma. In Fig. 1(c), this process is further illuminated by a second, 1 mW

HeNe laser. The zinc in the plasma reacts with water to form $Zn(OH)_2$, which chemically decays into ZnO nanoparticles. By changing the laser wavelength, number of laser shots and laser intensity, different morphologies of particles can be formed.

To monitor the precision of the ablation process, white light interferometric (WLI) optical profilometry (Filmetrics, Profilm3D) and optical microscopy (Leica, MC205) were used to perform quality assurance steps to monitor the zinc metal samples post-ablation, specifically to document the quality of crater formation and regularity of crater spacing on the sample.

(a) (b) (c) (d)

Figure 1: Experiment: (a) overall setup, (b) detail of ablation setup, (c) detail of plasma on zinc, (d) same process, illuminated by HeNe laser to illustrate particle plume

### *II. Nanoparticle Analysis*

The obtained nanoparticle suspension was concentrated, filtrated, ultra-sonicated, and centrifuged to attempt to reduce the aggregation and average diameter of zinc oxide nanoparticles. The diameter of particles in suspension was measured using the Dynamic Light Scattering (DLS) method (Malvern, ZEN3690). In DLS, the Brownian motion of suspended particles or molecules causes time-dependent scattering of laser light; analysis of these intensity fluctuations yields the velocity of the Brownian motion and hence the particle size using the Stokes-Einstein relationship. As a second method of confirmation of particle size, ZnO particles were transferred onto a polished aluminum stub by casting a drop of suspension over the stub and heating to dryness. Particles on the surface were imaged using Scanning Electron Microscopy (SEM) (JEOL, JSM-6060LV). Particle elemental composition (namely, zinc and oxygen) was confirmed during imaging using Energy Dispersal Spectroscopy (EDS) (Thermo Scientific, PF-NS6-UPG-C).

## Results

### *I. Ablation and Quality Control*

The ablated surfaces were analyzed using optical microscopy and WLI optical profilometry for better assurance of crater sizes and to provide quality control feedback for setting the parameters of the laser 2D stage. As shown in Table 3, the Arduino programming with 50×50×2 (steps) 10 rpm and 20 Hz produced good coverage of the surface during repetitive ablation. So, for further experiments, the same algorithm was used to get similar size particles and nanoparticles.

MINNESOTA UNDERGRADUATE SCHOLARS
Proceedings of the 9th Annual Minnesota State Conference of Undergraduate Scholarly and Creative Activity
and
St. Cloud State University Journal of Student Scholarship, Vol. 1, Special Issue 1, 2020
MINNESOTA STATE

Table 3: Quality Control of the Scanned Repetitive Ablation Process (Optical Profilometry)

| Steps | N/A | 50×50×5 | 200×200×5 | 50×50×2 |
|---|---|---|---|---|
| Laser | N/A | 20 Hz | 13 Hz | 20 Hz |
| Motor | N/A | 10rpm | 15rpm | 10rpm |
| 2D | 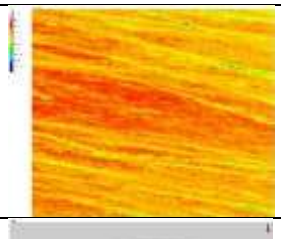 | 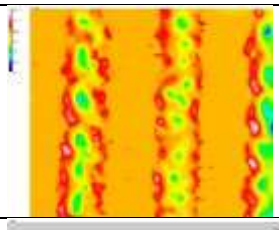 | 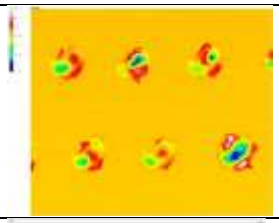 | 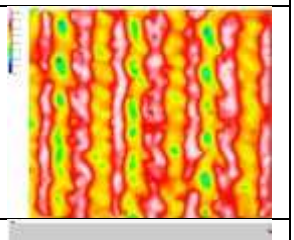 |
| 3D |  | 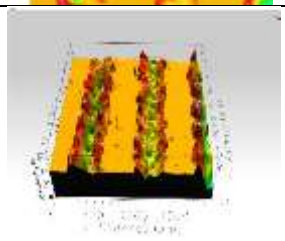 |  |  |

In the above 2D optical profilometry with 50×50×5 with 10 rpm, in each column of ablated zinc, the crater diameter is overlapped and there are no gaps but the gap between the columns is so large which reduces the probability of ablating more zinc oxide nanoparticles. For the steps in 200×200×5 with 15 rpm, the gaps between the rows and column are large, so less zinc is ablated, and less zinc oxide nanoparticles are produced. Hence, 50×50×2 steps at 10 rpm turn out to be the best because there is no gap in the rows and columns and crater diameter is not overlapped. In the 3D image the peaks and valleys can be easily seen.

The surface was also recorded via optical microscopy, as shown in Table 4:

Table 4: Quality Control of the Scanned Repetitive Ablation Process (Microscopic Images)

| Stage, $N_x \times N_y$ | 50×50 | 200×200 | 50×50 |
|---|---|---|---|
| Stage, # steps | 5 | 5 | 2 |
| Stage, motor set | 10 rpm | 15 rpm | 10 rpm |
| Laser pulse rate | 20 Hz | 13 Hz | 20 Hz |
| Low Microscope Magnification (bar = 1 mm) |  |  |  |
| High Microscope Magnification (bar = 200 µm) | 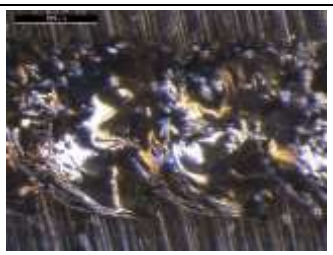 |  | 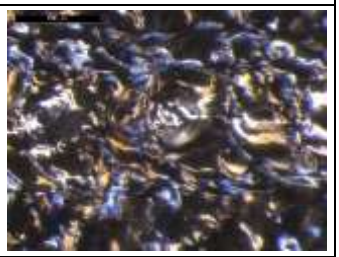 |

By looking into the crater size and surface quality of the microscopic images shown in Table 4, the Arduino algorithm was generated and refined. The ablated surface was inspected at both low and high magnifications (200 μm and 1 mm scale bars) as illustrated. The ablated pattern and surface using the parameters (50×50×2, 10rpm, 20 Hz) was best for use, since the ablated craters were not overlapped with each other, which we believe would result in maximizing the number and uniformity of particles ablated from the surface.

Our working hypothesis is that when the laser beam ablates the zinc metal surface, a dense zinc plasma region is produced at the liquid-solid interface. The presence of liquid medium surrounding the plasma, which is deionized water in this project, creates extra pressure on the plasma and restricts the expansion of plasma hence making it denser when compared to the plasma produced by conventional laser ablation (i.e., in air, without liquid). The plasma expands adiabatically at high velocity until it extinguishes when its temperature becomes too low to sustain its ionized state. After the disappearance of plasma, a cavitation bubble remains. As it continues to cool, its pressure drops. It may initially continue growing in size, driven by remnant pressure, but eventually it reaches a maximum size, then quickly collapses. The collapse of a cavitation bubble is a violent process that produces high temperature and pressure; hence it is possible that this phenomenon may contribute to the formation of ZnO nanoparticles. The relatively importance of the initial plasma-water interaction vs. the cavitation collapse in producing ZnO nanoparticles is presently unclear. In any event, zinc clusters produced in these events react with the water medium to form zinc hydroxide, $Zn(OH)_2$, and $Zn(OH)_2$ further decomposes to ZnO, following the reactions in Equations (5) and (6), respectively. [12,13]

$$Zn + 2H_20 \rightarrow Zn(OH)_2 + H_2 \qquad (5)$$

$$Zn(OH)_2 \rightarrow ZnO + H_2O \qquad (6)$$

Eventually, we would like to confirm the ratio of zinc to zinc oxide in our particle samples. That work is ongoing and has not yet been completed.

*II. Analysis of Nanoparticles via SEM and SEM-EDS*

The obtained nanoparticles were heated, concentrated, filtrated, ultra-sonicated, and centrifuged to attempt to reduce aggregation. Following casting of the suspension across an aluminum stub, and heating to dryness, SEM imaging with EDS was applied. SEM images of the raw zinc surface, and of the suspected ZnO nanoparticles, are shown in Figure 2. The particle size scale of produced nanoparticles was not yet analyzed in detail using SEM but appears to range from approximately 100-2000nm diameter.

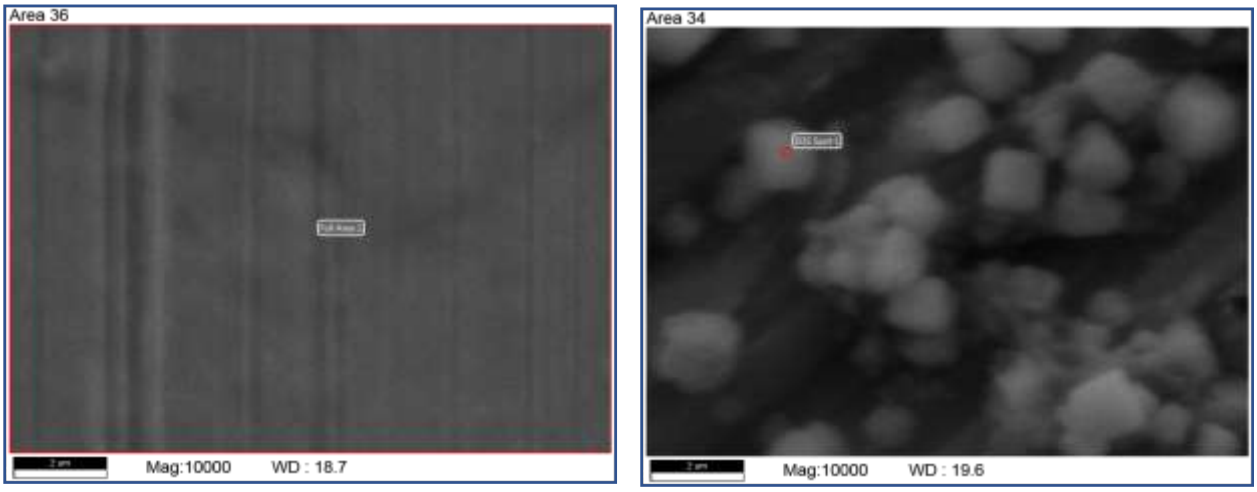


(a) (b)

Figure 2: SEM images of (a) unablated zinc surface and (b) ablated ZnO particles

Next, EDS analysis was performed on the raw zinc surface as a full area scan, as well as for selected points in the center of five ZnO particles, as shown in Fig. 3. Detailed results from the ZnO scans are shown in Table 3. While it is inadvisable and imprudent to rely on EDS for molecular identification, the data do support the claim that the particle composition includes zinc oxide and not merely zinc. The presence of aluminum in these data arises from the SEM sample stub upon which the particles were cast and dried.

Table 3: SEM-EDS Results for ZnO particles on an aluminum stub

| Element | Weight % | Atomic % | Error % | Net Int. |
|---|---|---|---|---|
| O K | 23.97 | 37.25 | 10.41 | 14.60 |
| Zn L | 13.54 | 5.15 | 11.47 | 4.48 |
| Al K | 62.49 | 57.60 | 5.75 | 39.84 |

The EDS scan of zinc is shown in Fig. 3(a), and for ZnO particles is shown in Fig. 3(b).

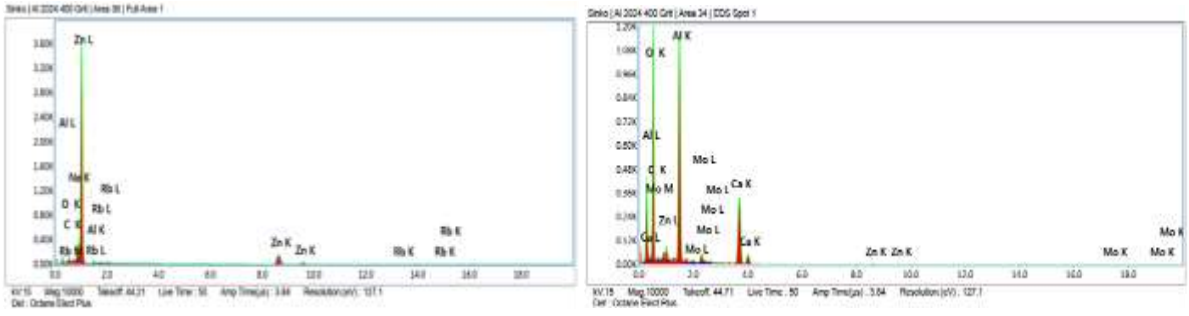

Figure 3: SEM-EDS data illustrating unablated zinc (a) and ablated particles (b)

Most worthwhile to note is the presence of oxygen in the ZnO particle data.

### *III. Analysis of Nanoparticle Size via DLS*

As a separate experiment, the size (diameter) of zinc oxide nanoparticles was measured in a water suspension by the DLS method. Fig. 4 shows the size distribution of the zinc-oxide particles with and without the addition of a surfactant over a range from 1-10000nm diameter. The vertical units are arbitrary, but indicate the frequency at which particles of a given size range are detected.

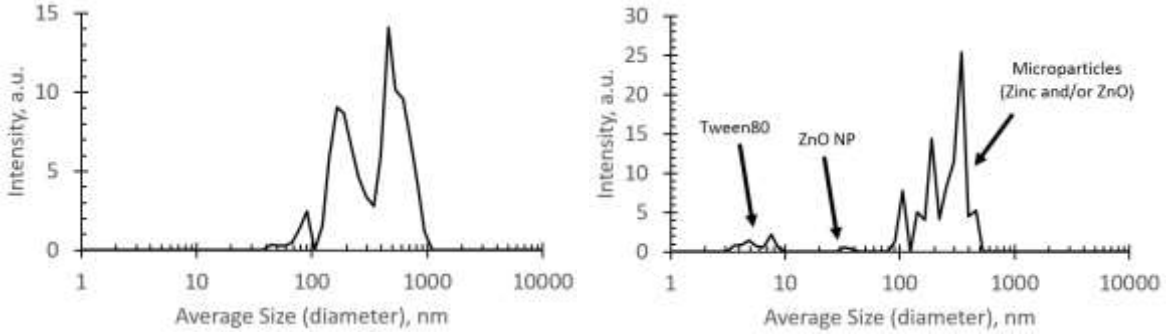


(a) (b)

Figure 4: DLS size distribution data: averages of 10 measurements, 10 scans each, each scan 300s length: (a) ZnO suspension with no surfactant, (b) ZnO suspension with Tween80 surfactant.

The polydispersity index (PDI) is a parameter which represents how wide the range of particle sizes extends. In these experiments, PDI increased from 0.73 to 0.93 with the addition of Tween80 surfactant. Most of this change is likely to arise from the introduction of the ~10 nm surfactant molecule into a suspension of generally 10-100× larger particles. The presence of ZnO nanoparticles can be assumptively discerned in the raw suspension between 40-100 nm in Fig. 4(a). The process was error-checked using separate DLS runs of water only (which yielded no usable data) and a suspension of Tween80 only (which is not shown, but confirmed the ~10nm size of this surfactant). With the addition of surfactant to the ablatant suspension, the ablated particles became resolvable at a smaller size range of roughly 30-100 nm as shown in Fig 4(b), with an apparent small peak around 35 nm, which may indicate the minimum size of ZnO particles achieved from this particular laser ablation method. While larger particles are present in both suspensions, it may be pointed out that the peaks of nearly 1 μm size are almost entirely removed in the presence of Tween80. Both features support our hypothesis that particle aggregation was distorting the initial results. Finally, we note that the ~10 nm Tween80 peak in Fig. 4(b) and in our control test with surfactant only (not shown) are consistent with the literature [8].

In looking ahead from these results, various factors affect ZnO nanoparticles; e.g., liquid medium, laser fluence (energy/area), pulse duration, laser power, ablation time and particle aggregation with respect to time. The higher the laser fluence, the more mass will be ablated, and we have some expectation that using a laser with a shorter pulse duration, lower wavelength, and higher energy per pulse could yield more monodisperse nanoparticles. One additional lesson learned from these experiments was that when the ablated zinc oxide particles are stored for long periods of time in suspension, they aggregate to form micrometer-scale clumps. The use of a surfactant such as Tween80 is likely to be necessary to achieve resolution of nanoparticles, but with our goal of achieving nanoparticles of <10 nm diameter, a surfactant significantly larger or smaller than Tween80 is likely needed to avoid masking such particles within the DLS peak of the surfactant. Future work on this project will surely include adjusting the laser focus to

determine if operation at higher or lower fluence will be better for production of small, monodisperse particles. If available, we hope to also explore using a laser with a much shorter pulse duration than 90 μs, as well as extend the experimentation into a lower wavelength, which would support a more vaporization-driven ablation process.

## Conclusions

In this study, a 2D motional stage was designed, built, and used to support pulsed laser ablative processing of a zinc plate immersed in water in an effort to generate zinc oxide nanoparticles. Ablated particles were collected and analyzed mainly using SEM imaging and SEM-EDS for dried particles, and the DLS method for an aqueous suspension of the ablatants. These efforts confirmed the presence of zinc oxide in the ablatants and measured the diameter of the nanoparticles at around 30-100 nm, with a peak around 35 nm. In our experiments, aggregation is one reason for not achieving particle size, less than (10±1) nm. Tween80 surfactant was used to attempt to disaggregate the suspended particles, and our DLS results suggest this approach met with success, although we did not produce significant numbers of ablated particles below 30nm in size. Hence, future work and technique on this research will strive to continue reducing the particle size, while reducing the range of ablated particle sizes.

## Acknowledgments

We would like to thank Dr. Christofer Nelson (Department of Physics & Astronomy, SCSU), who suggested this research, and also extend sincere gratitude to Dr. Sarah C. Petitto (Department of Chemistry & Biochemistry, SCSU) for her guidance and advice, particularly regarding safety and procedures for handling the surfactant chemicals. Education USA high school students Mercy Johnson and Vazira Ikxtiyorova assisted with experimental research in Summer 2019. The authors extend a special thank you to the St. Cloud State University Summer Undergraduate Research Fellowship and an SCSU Student Research Award, which helped us to purchase supplies and helped us financially to conduct the research.

## References

1. CRC Handbook of Chemistry and Physics, 69th ed., Eds. R. C. Weast, M. J. Astle, and W. H. Beyer, CRC Press: Boca Raton, 1988, (a) B-144, (b) B-42, (c) D-179, (d) E-15.
2. Y. Wang and N. Herron, "Nanometer-Sized Semiconductor Clusters: Materials Synthesis, Quantum Size Effects, and Photophysical Properties," *J. Phys. Chem.* **95**(2), pp. 525-532, 1991. doi:10.1021/j100155a009
3. Kuk Ki, K. et al. "Formation of ZnO Nanoparticles by Laser Ablation in Neat Water." *Chemical Physics Letters*, 511(3), 2011, pp. 116–120., doi:10.1016/j.cplett.2011.06.017.
4. C. B. Nelson, T. Zubkov, J. D. Adair, and M. Subir, "A synergistic combination of local tight binding theory and second harmonic generation elucidating surface properties of ZnO nanoparticles," *Phys. Chem. Chem. Phys.*, **44**, 29991-29997, 2017. doi:10.1039/c7cp06661a
5. M. Stafe, A. Marcu, N. Puscas, *Pulsed Laser Ablation of Solids*, Springer, New York, 2014, Ch. 3.3.1, pp 70-71.
6. S. C. Singh and R. Gopal, "Zinc Nanoparticles in Solution by Laser Ablation Technique," *Bull. Mater. Sci.* **30**(3), 291-293, 2007. doi:10.1007/s12034-007-0048-z.

7. R. K. Thareja and S. Shukla, "Synthesis and characterization of zinc oxide nanoparticles by laser ablation of zinc in liquid," *Appl. Surf. Sci.* **253**(22), pp. 8889-8895 (2007). doi:10.1016/j.apsusc.2007.04.088
8. M. Z. Hussain, R. Khan, R. Ali, and Y. Khan, "Optical Properties of Laser Ablated ZnO Nanoparticles Prepared with Tween-80," *Materials Letters* **122**, pp. 147–150, 2014. doi:10.1016/j.matlet.2014.02.022.
9. F. L. Pedrotti, L. S. Pedrotti, and L. M. Pedrotti, *Introduction to Optics, 3rd Ed.*, Pearson Prentice Hall: Upper Saddle River, 2007, Ch. 23-6 to 23-7, pp. 506-508.
10. W. S. M. Werner, K. Glantschnig, and C. Ambrosch-Draxl, "Optical Constants and Inelastic Electron-Scattering Data for 17 Elemental Metals," *J. Phys. Chem. Ref. Data* **38**(4), pp. 1013-1092, 2009.
11. A. T. Aldred and J. N. Pratt, "Vapor Pressures of Zinc, Cadmium, Antimony, and Thallium," *J. Chem & Eng. Data* **8**(3), 429-431, pp. (1963).
12. Sasaki, K. (2009), Liquid Phase Laser Ablation. 19th International Symposium on Plasma Chemistry; Bochum, 1-4.
13. J. N. Janice Low, W. Y. Wong, W. Rashmi, A. A. H. Kadhum, and A. B. Mohamad, "Synthesis of zinc oxide nanoparticles using liquid-phase laser ablation and its antibacterial activity," *J. Eng. Sci. & Tech.* **12**(2), pp. 29-43 (2017).